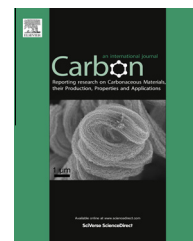


Available at www.sciencedirect.com

ScienceDirect

journal homepage: www.elsevier.com/locate/carbon

Carbon-coated graphene–Cr₂O₃ composites with enhanced electrochemical performances for Li-ion batteries

Wenbo Yue ^{a,*}, Shanshan Tao ^a, Jianmei Fu ^a, Ziqi Gao ^a, Yu Ren ^{b,*}

^a Beijing Key Laboratory of Energy Conversion and Storage Materials, College of Chemistry, Beijing Normal University, Beijing 100875, PR China

^b National Institute of Clean-and-Low-Carbon Energy, Beijing 102209, PR China

ARTICLE INFO

Article history:

Received 25 May 2013

Accepted 29 July 2013

Available online 13 August 2013

ABSTRACT

Graphene-based Cr₂O₃ composites are prepared and exhibit better electrochemical properties than free Cr₂O₃ particles without the graphene. The synthesis procedure consists of the direct growth of CrOOH on the surface of graphene and the subsequent thermal decomposition of CrOOH to Cr₂O₃. Moreover, the electrochemical properties of graphene-based Cr₂O₃ are further improved through carbon coating, and two strategies are developed. Interestingly, the carbon layers pyrolyzed from glucose on CrOOH can separate the particles on the graphene and limit their growth, while those on Cr₂O₃ merely cover the particles and cannot prevent particle aggregation. Consequently, compared to the latter carbon-coated composite, the former shows further improved electrochemical behavior.

© 2013 Elsevier Ltd. All rights reserved.

1. Introduction

Li-ion batteries (LIBs) have been widely used in portable electronic devices (e.g., laptops) due to their superior properties such as high energy density, long cycle life, no memory effect and environmental friendliness. Reversible Li-storage in several metals and metal oxides has been intensively studied in order to achieve high-capacity anode materials for LIBs [1,2]. The theoretical specific capacities of metal oxides (e.g., Co₃O₄, SnO₂) are usually 700–1000 mA h g⁻¹, much higher than that of the conventional graphite anode (~370 mA h g⁻¹) [3,4]. Notwithstanding, the synthesis and applications of Cr₂O₃ for LIBs are hardly investigated, even though Cr₂O₃ is one of the promising potential anode materials due to its high theoretical capacity (~1058 mA h g⁻¹) and relative low electromotive force value (1.085 V) [5,6]. On the other hand, like other metal oxide anodes, Cr₂O₃ is lack of practical use due to its low electrical conductivity and severe volume change during cycles, which result in a rapid capacity fading and the end of the

cycle life [7,8]. Several strategies have been developed to alleviate the volume change and increase the conductivity of the electrode, including the preparation of nanoscale materials (e.g., Cr₂O₃ nanoparticles) [9], hollow or mesoporous materials (e.g., mesoporous Cr₂O₃) [10,11], and carbon-based composites (e.g., carbon-coated Cr₂O₃) [12,13]. Recently, a novel two-dimensional carbon matrix (i.e., graphene) has attracted tremendous attention and is preferable to replace other carbon matrices (e.g., graphite) for supporting metal and metal oxides due to its excellent properties such as high electrical conductivities, unique mechanical properties and large specific surface areas [14,15]. The properties of active materials can be improved considerably through the synergistic effects of graphene and active materials [16,17]. For instance, graphene-based metal oxides usually exhibit excellent electrochemical performances as electrode materials for LIBs because the graphene substrate may enhance the electronic conductivity of the overall electrode and buffer the strain from the volume variation of metal oxides during

* Corresponding authors: Fax: +86 10 58802075.

E-mail addresses: wbyue@bnu.edu.cn (W. Yue), renyu@nicenergy.com (Y. Ren).

0008-6223/\$ - see front matter © 2013 Elsevier Ltd. All rights reserved.

<http://dx.doi.org/10.1016/j.carbon.2013.07.109>

lithiation and delithiation processes [18–21]. Therefore, graphene-based Cr_2O_3 can be expected to show enhanced performance for various applications such as gas sensors, LIBs, catalysts and magnetic materials [11,22,23]. Herein, we describe a novel strategy for the preparation of graphene-based Cr_2O_3 composites through a hydrothermal method followed by a subsequent thermal treatment. The overall synthesis procedure is illustrated in Fig. 1. First, the 2D graphene-based intermediate product (G-CrOOH) was formed under hydrothermal condition using $\text{Cr}(\text{NO}_3)_3$ as the precursor, and urea as the precipitant. Subsequently, the graphene-based Cr_2O_3 (G- Cr_2O_3) was formed after calcination under N_2 protection. Compared to free Cr_2O_3 particles without the graphene, the nanoscale Cr_2O_3 particles decorated on the graphene surface exhibited higher reversible capacity, better cycle performance and rate capability.

It is also important to note that the particles on the graphene surface are still prone to disintegrate, and the graphene-metal oxide hybrids may randomly aggregate, leading to a decreased electrochemical performance. To overcome these drawbacks, the graphene-based metal oxides are further confined within a carbon layer through the carbonization of glucose or phenol [24,25]. The resulting 2D sandwich-like structure may protect the particles on the graphene against disintegration and buffer the strain induced by the volume expansion during cycles. Moreover, the carbon shells can also keep the overall electrode highly conductive and active in Li storage, but the aggregation of particles on the graphene is still inevitable [24,25]. Herein, the as-synthesized graphene-based Cr_2O_3 were further coated by carbon layers pyrolyzed from glucose, and along that approach, two strategies were developed (Fig. 1). Unlike graphene-based SnO_2 or TiO_2 previously reported [26–29], graphene-based Cr_2O_3 cannot be directly formed using the hydrothermal method. Therefore, the carbon source (i.e., glucose) can be first attached to either G-CrOOH or G- Cr_2O_3 under hydrothermal condition and then carbonized by heat treatment in an inert atmosphere. The resulting carbon-coated products (G- Cr_2O_3 -C1 or G- Cr_2O_3 -C2) showed enhanced electrochemical performance in compari-

son with G- Cr_2O_3 due to the additional carbon layer protection. Furthermore, the Cr_2O_3 particles in G- Cr_2O_3 -C1 were highly dispersed by carbon shells, while the particles including the aggregation were coated by carbon layers in G- Cr_2O_3 -C2. Apparently, G- Cr_2O_3 -C1 showed further improved performance in terms of the reversible capacity and cycling stability than G- Cr_2O_3 -C2.

2. Experimental

2.1. Sample preparation

Graphene oxide (GO) was synthesized from natural graphite powders by a modified Hummer's method (see Supporting Information for details) [30]. The graphene-based Cr_2O_3 composites were synthesized by a hydrothermal method followed by a subsequent thermal treatment. In brief, 0.20 g of $\text{Cr}(\text{NO}_3)_3 \cdot 9\text{H}_2\text{O}$ was firstly added into 80 mL of GO dispersion solution (0.5 g L^{-1}), and after stirring for 0.5 h, 0.14 g of urea was added into the above solution. After stirring for another 0.5 h, this solution was transferred into the 100 mL Teflon lined stainless steel autoclaves and heated at $120 \text{ }^\circ\text{C}$ for 5 h. The resulting G-CrOOH was collected by centrifugation, washed with water, and dried at $40 \text{ }^\circ\text{C}$ in vacuum. Subsequently, the black powder was further heated under N_2 protection at $650 \text{ }^\circ\text{C}$ for 2 h to obtain G- Cr_2O_3 . In addition, free Cr_2O_3 particles without graphene (denoted as F- Cr_2O_3) was also prepared by calcination of G- Cr_2O_3 at $800 \text{ }^\circ\text{C}$ for 2 h in air.

The carbon-coated graphene- Cr_2O_3 composites were synthesized through the carbonization of glucose on the surface of graphene-based Cr_2O_3 . In brief, the obtained G-CrOOH or G- Cr_2O_3 was dispersed in 80 mL of distilled water by ultrasonication for 20 min, and then 0.30 g of glucose was added into the above solution. After stirring for 0.5 h, this solution was transferred into the 100 mL Teflon lined stainless steel autoclaves and heated at $160 \text{ }^\circ\text{C}$ for 10 h. The precipitate was collected by centrifugation, washed with water, dried in vacuum, and then heated under N_2 protection at $650 \text{ }^\circ\text{C}$ for 2 h to obtain G- Cr_2O_3 -C1 or G- Cr_2O_3 -C2.

2.2. Sample characterization

Specimens were initially characterized using X-ray diffraction (XRD) on a Phillips X'pert Pro MPD diffractometer with Cu K_α radiation. The Fourier transform infrared (FT-IR) spectra were recorded on a Nicolet-380 Fourier transform infrared spectrometer in the range of $400\text{--}4000 \text{ cm}^{-1}$. X-ray photoelectron (XPS) spectra were recorded on a Shimadzu Axis Ultra spectrometer with an $\text{Mg K}_\alpha = 1253.6 \text{ eV}$ excitation source. The thermogravimetric analysis (TGA) was performed on a NETZSCH STA 409 PC/PG thermal analyzer and carried out in air at a heating rate of $5 \text{ }^\circ\text{C}/\text{min}$. Further characterization was performed by using transmission electron microscopy (TEM), high-resolution TEM (HRTEM) on a JEOL JEM-2011 electron microscope operated at 200 kV, scanning electron microscope (SEM) on a JEOL Ltd. JSM-6700F electron microscope at an accelerating voltage of 1 kV. Energy-dispersive X-ray microanalysis (EDX) attached in electron microscope was used to qualitatively determine the present elements.

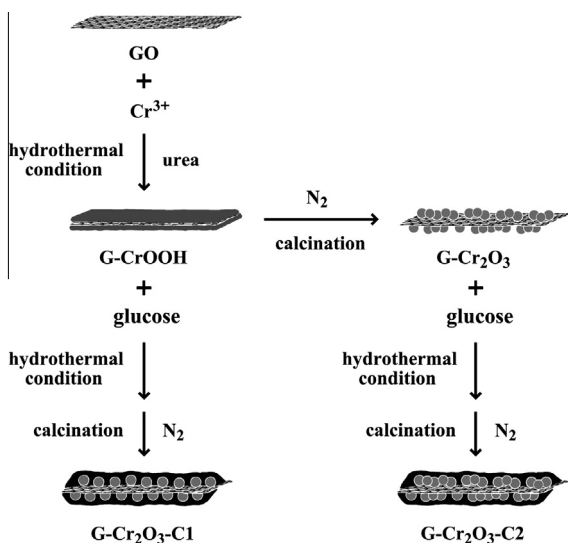


Fig. 1 – Illustration of the synthesis routes for G- Cr_2O_3 , G- Cr_2O_3 -C1 and G- Cr_2O_3 -C2.

2.3. Electrochemical measurements

For electrochemical characterization, the composite electrodes were fabricated by mixing the synthesized samples, acetylene black and polyvinylidene difluoride (PVDF) dissolved in N-methyl-2-pyrrolidone (NMP) in a weight ratio of 70:15:15. The mixed slurry was pressed onto a copper foil and dried at 110 °C in vacuum for 24 h. Cell assembly was carried out in an Ar-filled glove box. The electrolyte was 1 M solution of LiPF₆ in EC:DEC:DMC with volume ratio 1:1:1. Electrochemical performances were measured with a CR2032-type coin cell with Li metal as the negative electrode. The galvanostatic charge–discharge performance was measured with a LAND test system at room temperature, and the voltage range was from 0.01 to 3.0 V (versus Li/Li⁺), with a constant current of 0.1–1 C (1 C = 1058 mA g⁻¹). Cyclic voltammetry (CV) tests were performed between 0.01 and 3.0 V with a scan rate of 0.2 mV s⁻¹, and the electrochemical impedance spectroscopy (EIS) was carried out in the frequency range from 100 kHz to 10 MHz on a Princeton PAR-STAT 4000 electrochemical station.

3. Results and discussion

3.1. Structure and morphology

The crystalline phases of Cr-containing composites were firstly identified by XRD. Fig. S1 shows the XRD pattern of G-CrOOH. Only four weak and broad peaks could be distinguished in the XRD pattern, and indexed to the rhombohedral HCrO₂ structure (space group *R*-3*m*, *a* = 0.2977 nm, and *c* = 1.3362 nm) [31], indicating the formation of amorphous-like CrOOH on the graphene. Moreover, the feature diffraction peak for GO at ca. 11° disappears in the XRD patterns of G-CrOOH, implying that GO was possibly reduced to graphene. Fig. 2 shows the XRD patterns of F-Cr₂O₃, G-Cr₂O₃, G-Cr₂O₃-C1 and G-Cr₂O₃-C2. The feature diffraction peaks in each XRD pattern corresponded to the (012), (104), (110), (113), (024), (116), (214) and (300) planes of rhombohedral Cr₂O₃ (space group *R*-3*c*, *a* = 0.4957 nm, and *c* = 1.3592 nm), deducing that amorphous CrOOH had been completely converted to crystalline Cr₂O₃ under thermal treatment. Moreover, the GO peak was also absent in the XRD pattern of G-Cr₂O₃ and the conventional stacking peak of graphene nanosheets at ca. 26° could be appreciably detected, proving the formation

of graphene-based Cr₂O₃. The average size of Cr₂O₃ nanoparticles calculated from XRD patterns was ~25 nm for G-Cr₂O₃, slightly smaller than that for F-Cr₂O₃ (~38 nm), and larger than that for G-Cr₂O₃-C1 (~11 nm). The average size of Cr₂O₃ nanoparticles for G-Cr₂O₃-C2 was ~22 nm, similar to that for G-Cr₂O₃.

The reduction degree of GO in composites as electrodes for LIBs was very important and further characterized by FT-IR and XPS. Fig. 3A shows the FT-IR spectra of GO and G-Cr₂O₃. In the FT-IR spectrum of GO, the absorption bands at 1734, 1374, 1227, 1061 and 1624 cm⁻¹ were assigned to the stretching vibrations of C=O, O–H, C–OH, C–O groups and the skeletal vibration of C=C from unoxidized graphitic domains, respectively [32]. In contrast, C=O, C–O and O–H bands disappeared in the FT-IR spectra of G-Cr₂O₃, demonstrating that the oxygen-containing functionalities of GO were almost removed. Furthermore, the characteristic absorption peaks of Cr₂O₃ at 557 and 617 cm⁻¹ were present, indicating the presence of Cr₂O₃ in the G-Cr₂O₃ sample [33]. Fig. 3B shows a survey XPS spectrum from G-Cr₂O₃, and three elements (C, O and Cr) were detected. The peaks located at ca. 284, 532, 576.9 and 586.4 eV corresponded to the binding energy of C 1s, O 1s, Cr 2p_{3/2} and Cr 2p_{1/2} (inset of Fig. 3B) [34], respectively, suggesting that the G-Cr₂O₃ sample consisted of graphene and Cr₂O₃. The high reduction degree of GO in G-Cr₂O₃ was also confirmed by the fine spectrum of C 1s (Fig. 3C). The C 1s peak could further be divided into four peaks located at 284.7, 286.5, 287.6, 288.9 eV, which corresponded to C–C, C–O, C=O and O–C=O groups, respectively [32]. Noticeably, the peaks related to the oxidized groups were so weak, also suggesting the complete reduction of GO. The loading of Cr₂O₃ in each composite was accurately determined by TGA. According to the TGA curves from these Cr₂O₃-containing composites (Fig. 3D), the Cr₂O₃ contents were ca 51.2 wt% in G-Cr₂O₃, 39.6 wt% in G-Cr₂O₃-C1, and 41.9 wt% in G-Cr₂O₃-C2. Besides, the results also showed that the carbon-coated composites (C1 and C2) contained ca. 18–22 wt% carbon derived from glucose.

The morphology and structure of Cr-containing composites were elucidated by SEM and TEM. Figs. 4 and S2 show the TEM and SEM images of G-CrOOH, G-Cr₂O₃, G-Cr₂O₃-C1 and G-Cr₂O₃-C2. According to the TEM and SEM images of G-CrOOH (Figs. 4A and S2A), the wrinkled graphene nanosheet was observed and no distinct particles were decorated on its surface. Moreover, three elements (C, O, and Cr) were detected by EDX (inset of Fig. S2A), suggesting the formation

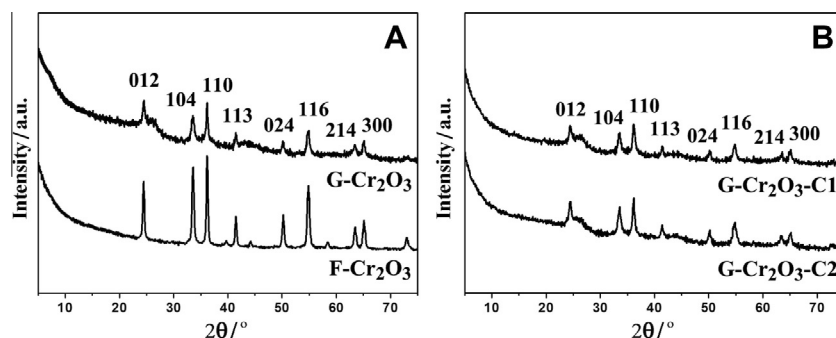


Fig. 2 – XRD patterns of (A) F-Cr₂O₃, G-Cr₂O₃ and (B) G-Cr₂O₃-C1, G-Cr₂O₃-C2, respectively.

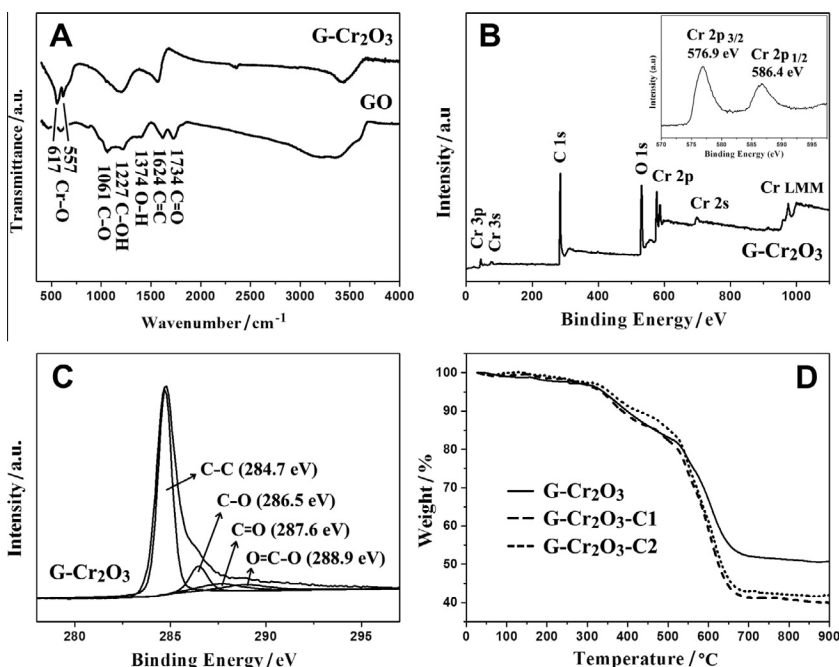


Fig. 3 – (A) FT-IR spectra of GO and G-Cr₂O₃. (B, C) survey and C 1s XPS spectra of G-Cr₂O₃. (D) TGA curves of G-Cr₂O₃, G-Cr₂O₃-C1 and G-Cr₂O₃-C2. The inset of (B) is Cr 2p XPS spectrum of G-Cr₂O₃.

of amorphous-like CrOOH on the graphene. After calcination under N₂ protection, crystalline Cr₂O₃ nanoparticles were formed on the graphene, and meanwhile, some large particles and agglomerates were also observed (Figs. 4B and S2B), which might result from the CrOOH formed in the solution. In contrast, few large particles or agglomerates were discerned in the TEM and SEM images of G-Cr₂O₃-C1 (Figs. 4C and S2C), implying that the formed carbon associated with Cr₂O₃ particles might tackle the particle growth and aggregation. The crystalline and particle size of Cr₂O₃ in G-Cr₂O₃ and G-Cr₂O₃-C1 were further determined by HRTEM. The HRTEM images (Fig. 4E and F) revealed that the nanoparticles exhibit well-defined lattice spacing of ca. 0.216 and 0.248 nm, corresponding to the (113) and (110) planes of Cr₂O₃ crystal. In addition, the Cr₂O₃ nanoparticles with diameters in the range of ca. 5–10 nm were randomly formed on the graphene, and the aggregation was ineluctable (Fig. 4E), whereas the nanoparticles with sizes of ca. 2–5 nm were highly dispersed by additional carbons on the graphene (Fig. 4F). The TEM image of G-Cr₂O₃-C2 (Fig. 4D) was not much different from that of G-Cr₂O₃, indicating that the carbon layers formed after the formation of Cr₂O₃ had little influence on the size and aggregation of Cr₂O₃ particles. Additionally, the carbon layers on the surface of graphene-Cr₂O₃ could be appreciably distinguished based on the SEM observation (Fig. S2D). To further confirm the presence of carbon coating, EDX was performed to identify the elements present in G-Cr₂O₃, G-Cr₂O₃-C1, and G-Cr₂O₃-C2 samples. More than five nanosheets for each sample were selected to be characterized. The intensity ratios of C peak to Cr peak for G-Cr₂O₃-C1 and G-Cr₂O₃-C2 were much higher than that for G-Cr₂O₃. The typical EDX spectra of these samples were shown in Fig. S3. The weight contents of carbon were ~47.9 wt% for G-Cr₂O₃, ~58.7 wt% for G-Cr₂O₃-C1 and ~60.6 wt% for G-Cr₂O₃-C2, respectively, which were

consistent with the TGA result. The additional carbon might be ascribed to the carbon layer derived from the glucose.

3.2. Electrochemical performance

To identify the electrochemical reactions during cycles, cyclic voltammograms (CV) of F-Cr₂O₃, G-Cr₂O₃, G-Cr₂O₃-C1, and G-Cr₂O₃-C2 electrodes were characterized in the range of 0.01–3.0 V. Fig. S4A shows the CV profiles of F-Cr₂O₃ in the 1st, 2nd and 5th scanning cycles. In the first cathodic sweep, it exhibited a distinct reduction peak at ~0.47 V, which was related to the first electrochemical process of Cr₂O₃, including the reduction of Cr₂O₃-Cr and the formation of the solid electrolyte interface (SEI) layer. In the first anodic sweep, two peaks observed at ~1.03 V and ~2.16 V indicated the partial decomposition of the SEI layer and the reoxidation of Cr [11,13]. In the second and fifth cycles, the reduction peak shifted to a higher potential at ~0.90 V, and the electrochemical reactions were reversible. Fig. S4B shows the 1st, 2nd and 5th CV curves of G-Cr₂O₃. The peak corresponding to the reduction of Cr₂O₃ appeared at ~0.65 V in the first cathodic sweep, and shifted to a potential at ~0.78 V in subsequent cycles. Another reduction peak was observed at ~0.02 V, which was assigned to the insertion of Li⁺ into graphene (the peak at ~0.02 V in the CV curves of F-Cr₂O₃ might be attributed to the presence of acetylene black in the cells). Fig. S4C, D show CV curves of G-Cr₂O₃-C1 and G-Cr₂O₃-C2, which were similar to the curves of G-Cr₂O₃, indicating the same electrochemical reactions. The electrochemical performances of these Cr₂O₃-containing composites were also evaluated by galvanostatic measurements. Fig. 5A shows the first cycle charge-discharge voltage profiles for F-Cr₂O₃, G-Cr₂O₃ and G-Cr₂O₃-C2 samples at a constant current density of 0.1 C. Only one plateau was identified in the discharge process, corresponding

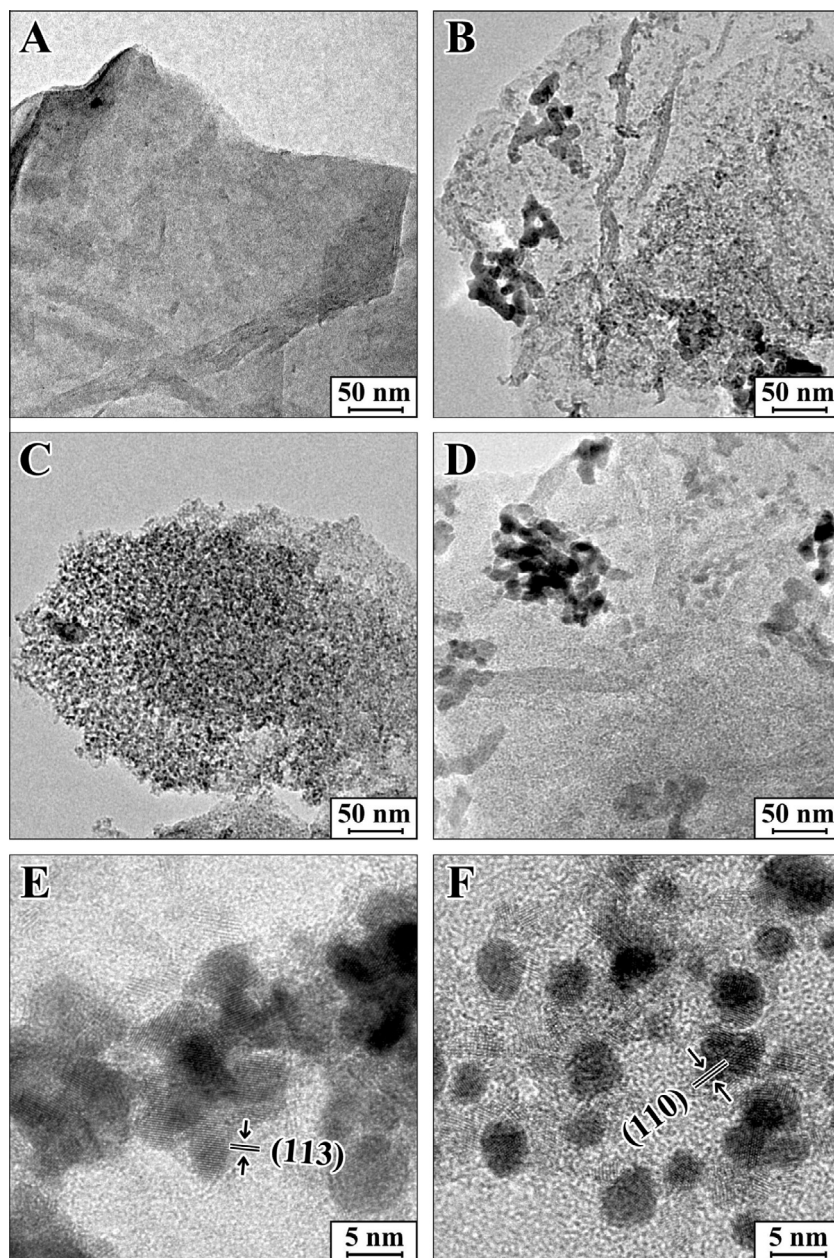


Fig. 4 – TEM images of (A) G-CrOOH, (B) G-Cr₂O₃, (C) G-Cr₂O₃-C1, (D) G-Cr₂O₃-C2 and HRTEM images of (E) G-Cr₂O₃, (F) G-Cr₂O₃-C1, respectively.

to the transformation of Cr₂O₃ and Li⁺ to Cr and Li₂O, which is in good agreement with the Li-storage mechanism of other Cr₂O₃-based anodes [6,10]. The first charge and discharge capacities were ca. 763.9 and 1114.2 mA h g⁻¹ for G-Cr₂O₃, ca. 894.5 and 1234.1 mA h g⁻¹ for G-Cr₂O₃-C2, much higher than those of F-Cr₂O₃ (ca. 371.3 and 732.0 mA h g⁻¹), which may be attributed to the high electrical conductivity of graphene and the dispersion of Cr₂O₃ nanoparticles on the graphene. Additionally, the first discharge capacities of G-Cr₂O₃ and G-Cr₂O₃-C2 were also higher than the theoretical capacity of Cr₂O₃, which can be ascribed to the SEI layer formation on the surface of composites [3,4]. Fig. 5B shows the cycle performances of F-Cr₂O₃, G-Cr₂O₃ and G-Cr₂O₃-C2 at 0.1 C. Without the graphene substrate, the capacity of F-Cr₂O₃ decreased

rapidly to ~100 mA h g⁻¹ after only 10 cycles. On the contrary, G-Cr₂O₃ showed good cycling stability and high stable reversible capacities, e.g., ~450 mA h g⁻¹ after 100 cycles, which was still higher than the theoretical capacity of graphite (~370 mA h g⁻¹). As expected, the graphene substrate effectively buffered the strain from the volume variation of Cr₂O₃, leading to the improvement of cycle performance of G-Cr₂O₃. Moreover, according to the previous report [35], the C–O–Cr bridge in the composite might also contribute to the improvement of the electrochemical performance. Fig. S5 shows the cycle performance of graphene prepared under the same condition but without Cr₂O₃. The capacity of graphene after 100 cycles was ~330 mA h g⁻¹, much smaller than that of G-Cr₂O₃ (~450 mA h g⁻¹). Thus, the capacity contrib-

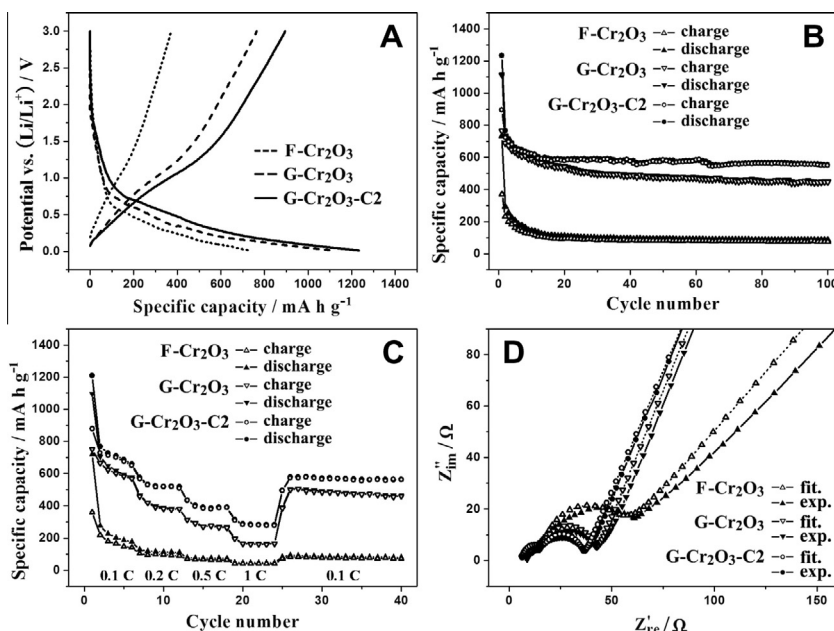


Fig. 5 – (A) the first cycle charge–discharge curves for F-Cr₂O₃, G-Cr₂O₃ and G-Cr₂O₃-C2 at 0.1 C in the voltage range 0.01–3.0 V. **(B, C)** the charge and discharge capacities as a function of cycle numbers for F-Cr₂O₃, G-Cr₂O₃ and G-Cr₂O₃-C2 at 0.1 C and 0.1–1 C. **(D)** the electrochemical impedance spectra of F-Cr₂O₃, G-Cr₂O₃ and G-Cr₂O₃-C2 after 3 cycles.

uted by the Cr₂O₃ should be ~570 mA h g⁻¹ owing to the weight content of Cr₂O₃ (~51.2 wt%) in G-Cr₂O₃. Compared to G-Cr₂O₃, the carbon-coated composites, G-Cr₂O₃-C2, exhibited better cycle performance and higher reversible capacities, e.g., ~550 mA h g⁻¹ after 100 cycles. The improved electrochemical performance of G-Cr₂O₃-C2 can be assigned to the synergistic effects of the graphene, carbon layer, and Cr₂O₃. Namely, the combination of graphene nanosheets and carbon layers gives rise to a high electrical conductivity of the overall electrode and accommodate the volume expansion of Cr₂O₃ particles during the cycling [24,25]. Fig. 5C shows the rate capabilities of these three samples evaluated by measurement of them at 0.1–1 C. The capacity of F-Cr₂O₃ decreased rapidly with the increase of the current density, while G-Cr₂O₃ showed better rate capability than F-Cr₂O₃. G-Cr₂O₃-C2 exhibited highest capacities among these three samples, even at a high current density of 1 C, which was as high as ~280 mA h g⁻¹, indicating its good rate capabilities. Additionally, a capacity of ~560 mA h g⁻¹ was retained after 40 cycles when the current density recovered to 0.1 C, also implying its good cycling stability. The EIS measurements of these samples were also carried out to gain insight into the superior electrochemical behavior of carbon-coated graphene–Cr₂O₃. The equivalent circuit model was shown in Fig. 6D to represent the internal resistances of these batteries [20,24]. The symbols of R_e, R_f, C_f, R_{ct}, C_d, and Z_w denoted the electrolyte resistance, the resistance and capacitance of the SEI film, the charge transfer resistance, the double layer capacitance, and the Warburg impedance, respectively [25,32]. The Nyquist plots of F-Cr₂O₃, G-Cr₂O₃ and G-Cr₂O₃-C2 samples (Fig. 5D) showed two semicircles in the high and medium frequency range, and a sloping line in the low

frequency range, corresponding to the migration of the Li⁺ ions through the SEI film (R_f), the charge-transfer impedance (R_{ct}) on the electrode/electrolyte interface, and the diffusion of the Li⁺ ions in the bulk of the electrode (Z_w). The Warburg component was further substituted with the constant phase element (CPE), which can describe more accurately the deviations in the sloping line [36]. Note that the fitting curves (fit.) was in accord with the curves obtained in the experiment (exp.). The radius of the medium-frequency semicircle for F-Cr₂O₃ was much larger than that for G-Cr₂O₃ or G-Cr₂O₃-C2. Apparently, the R_{ct} values of G-Cr₂O₃ (~27.9 Ω) and G-Cr₂O₃-C2 (~21.4 Ω) were much smaller than that of F-Cr₂O₃ (~48.2 Ω) due to the excellent conductivity of graphene. On the other hand, compared to G-Cr₂O₃, G-Cr₂O₃-C2 possessed lower charge-transfer impedance, validating that the introduced carbon can improve the electrical conductivity of the overall electrode, and thereby resulted in the improvement of the electrochemical performances in LIBs.

The electrochemical performance of G-Cr₂O₃-C1 including the cycle performance, rate capability and electrochemical impedance were also evaluated and shown in Fig. 6. It is striking to note that G-Cr₂O₃-C1 showed better cycle performance and rate capability than G-Cr₂O₃-C2. For instance, a reversible capacity up to ~630 mA h g⁻¹ could be maintained after 100 cycles without an apparent capacity loss (Fig. 6A), and a reversible capacity of ~315 mA h g⁻¹ could remain at 1 C (Fig. 6B). Besides, the charge-transfer resistance of G-Cr₂O₃-C1 after 3 cycles (Fig. 6C) was ~18.1 Ω, even lower than that of G-Cr₂O₃-C2 (~21.4 Ω). A possible explanation is that the growth of Cr₂O₃ nanoparticles on the graphene was limited by the surrounding carbon, benefiting the fabrication of separated small Cr₂O₃ particles, and avoiding the aggregation. Furthermore, the car-

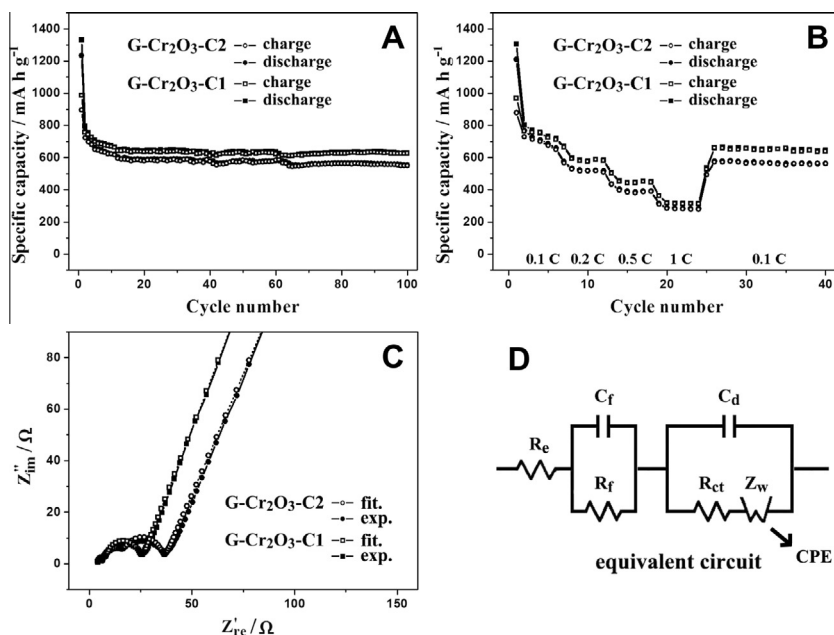


Fig. 6 – (A, B) the charge and discharge capacities as a function of cycle numbers for G-Cr₂O₃-C1 and G-Cr₂O₃-C2 at 0.1 C and 0.1–1 C. (C) the electrochemical impedance spectra of G-Cr₂O₃-C1 and G-Cr₂O₃-C2 after 3 cycles. (D) the equivalent circuit model (R_e : electrolyte resistance, R_f and C_f : the resistance and capacitance of the SEI film, R_{ct} : charge transfer resistance, C_d : double layer capacitance, Z_w : Warburg impedance).

bon layers covering Cr₂O₃ particles might restrain the volume change of Cr₂O₃. These factors contribute to the enhanced electrochemical performance of G-Cr₂O₃-C1.

4. Conclusions

A novel graphene-based Cr₂O₃ composite was synthesized using a hydrothermal method followed by a subsequent thermal treatment. Although this graphene-based Cr₂O₃ exhibited better electrochemical performance in comparison with pure Cr₂O₃, the exposed particles on the graphene were still prone to disintegrate or aggregate, leading to a slightly capacity fading. Thus two strategies were developed to prepare carbon-coated graphene-Cr₂O₃, which showed further enhanced electrochemical performances due to the carbon layer protection. Moreover, the carbon layers formed simultaneously with Cr₂O₃ particles could separate the particles and limit their growth, whereas the carbon layers formed after the formation of Cr₂O₃ particles merely covered the particles and could not prevent particle aggregation. As a result, the former carbon-coated composite showed further improved electrochemical properties compared to the latter composite, such as higher reversible capacity, better cycle performance and rate capability. This novel strategy may offer an effective technique for the preparation of other carbon-coated graphene-based composites for energy storage devices.

Acknowledgement

This work was financially supported by National Natural Science Foundation of China (21101014 and 21273022).

Appendix A. Supplementary data

Supplementary data associated with this article can be found, in the online version, at <http://dx.doi.org/10.1016/j.carbon.2013.07.109>.

REFERENCES

- [1] Wang ZY, Zhou L, Lou XW. Metal oxide hollow nanostructures for lithium-ion batteries. *Adv Mater* 2012;24(14):1903–11.
- [2] Zhao NQ, Wu S, He CN, Wang ZY, Shi CS, Liu EZ, et al. One-pot synthesis of uniform Fe₃O₄ nanocrystals encapsulated in interconnected carbon nanospheres for superior lithium storage capability. *Carbon* 2013;57:130–8.
- [3] Yue WB, Lin ZZ, Jiang SH, Yang XJ. Preparation of graphene-encapsulated mesoporous metal oxides and their application as anode materials for lithium-ion batteries. *J Mater Chem* 2012;22(32):16318–23.
- [4] Jiang SH, Yue WB, Gao ZQ, Ren Y, Ma H, Zhao XH, et al. Graphene-encapsulated mesoporous SnO₂ composites as high performance anodes for lithium-ion batteries. *J Mater Sci* 2013;48(10):3870–6.
- [5] Hu J, Li H, Huang XJ. Cr₂O₃-based anode materials for Li-ion batteries. *Electrochem Solid-State Lett* 2005;8(1):A66–9.
- [6] Dupont L, Grugeon S, Laruelle S, Tarascon JM. Structure, texture and reactivity versus lithium of chromium-based oxides films as revealed by TEM investigations. *J Power Sources* 2007;164(2):839–48.
- [7] Nethravathi C, Viswanath B, Michael J, Rajamath M. Hydrothermal synthesis of a monoclinic VO₂ nanotube-graphene hybrid for use as cathode material in lithium ion batteries. *Carbon* 2012;50(13):4839–46.

- [8] Yue WB, Jiang SH, Huang WJ, Gao ZQ, Li J, Ren Y, Zhao XH, Yang XJ. Sandwich-structural graphene-based metal oxides as anode materials for lithium-ion batteries. *J Mater Chem A* 2013;1(23):6928–33.
- [9] Hu J, Li H, Huang XJ, Chen LQ. Improve the electrochemical performances of Cr_2O_3 anode for lithium ion batteries. *Solid State Ionics* 2006;177(26–32):2791–9.
- [10] Dupont L, Laruelle S, Grugeon S, Dickinson C, Zhou WZ, Tarascon JM. Mesoporous Cr_2O_3 as negative electrode in lithium batteries: TEM study of the texture effect on the polymeric layer formation. *J Power Sources* 2008;175(1):502–9.
- [11] Liu H, Du XW, Xing XR, Wang GX, Qiao SZ. Highly ordered mesoporous Cr_2O_3 materials with enhanced performance for gas sensors and lithium ion batteries. *Chem Commun* 2012;48(6):865–7.
- [12] Jiang LY, Xin S, Wu XL, Li H, Guo YG, Wan LJ. Non-sacrificial template synthesis of Cr_2O_3 -C hierarchical core/shell nanospheres and their application as anode materials in lithium-ion batteries. *J Mater Chem* 2010;20(35):7565–9.
- [13] Guo BK, Chi MF, Sun XG, Dai S. Mesoporous carbon- Cr_2O_3 composite as an anode material for lithium ion batteries. *J Power Sources* 2012;205:495–9.
- [14] Geim AK, Novoselov KS. The rise of graphene. *Nat Mater* 2007;6(3):183–91.
- [15] Novoselov KS, Geim AK, Morozov SV, Jiang D, Katsnelson MI, Grigorieva IV, et al. Two-dimensional gas of massless Dirac fermions in graphene. *Nature* 2005;438(7065):197–200.
- [16] Li N, Geng ZF, Cao MH, Ren L, Zhao XY, Liu B, et al. Well-dispersed ultrafine Mn_3O_4 nanoparticles on graphene as a promising catalyst for the thermal decomposition of ammonium perchlorate. *Carbon* 2013;54:124–32.
- [17] Gao LN, Yue WB, Tao SS, Fan LZ. Novel strategy for preparation of graphene-Pd, Pt composite, and its enhanced electrocatalytic activity for alcohol oxidation. *Langmuir* 2013;29(3):957–64.
- [18] Zhai DY, Li BH, Du HD, Gao GY, Gan L, He YB, et al. The preparation of graphene decorated with manganese dioxide nanoparticles by electrostatic adsorption for use in supercapacitors. *Carbon* 2012;50(14):5034–43.
- [19] Hu T, Sun X, Sun HT, Yu MP, Lu FY, Liu CS, et al. Flexible free-standing graphene- TiO_2 hybrid paper for use as lithium ion battery anode materials. *Carbon* 2013;51:322–6.
- [20] Yue WB, Yang S, Ren Y, Yang XJ. In situ growth of Sn, SnO on graphene nanosheets and their application as anode materials for lithium-ion batteries. *Electrochim Acta* 2013;92:412–20.
- [21] Yue WB, Yang S, Liu YL, Yang XJ. A facile synthesis of mesoporous graphene-tin composites as high-performance anodes for lithium-ion batteries. *Mater Res Bull* 2013;48(4):1575–80.
- [22] Tamiolakis I, Lykakis IN, Katsoulidis AP, Stratakis M, Armatas GS. Mesoporous Cr_2O_3 -phosphomolybdic acid solid solution frameworks with high catalytic activity. *Chem Mater* 2011;23(18):4204–11.
- [23] Lei SJ, Peng XM, Liang ZH, Li XP, Wang CY, Cheng BC, et al. Self-template formation and properties study of Cr_2O_3 nanoparticle tubes. *J Mater Chem* 2012;22(4):1643–51.
- [24] Zhang CF, Peng X, Guo ZP, Cai CB, Chen ZX, Wexler D, et al. Carbon-coated SnO_2 /graphene nanosheets as highly reversible anode materials for lithium ion batteries. *Carbon* 2012;50(5):1897–903.
- [25] Su YZ, Li S, Wu DQ, Zhang F, Liang HW, Gao PF, et al. Two-dimensional carbon-coated graphene/metal oxide hybrids for enhanced lithium storage. *ACS Nano* 2012;6(9):8349–56.
- [26] Ding SJ, Luan DY, Boey FYC, Chen JS, Lou XW. SnO_2 nanosheets grown on graphene sheets with enhanced lithium storage properties. *Chem Commun* 2011;47(25):7155–7.
- [27] Ding SJ, Chen JS, Luan DY, Boey FYC, Madhavi S, Lou XW. Graphene-supported anatase TiO_2 nanosheets for fast lithium storage. *Chem Commun* 2011;47(20):5780–2.
- [28] Chen JS, Wang ZY, Dong XC, Chen P, Lou XW. Graphene-wrapped TiO_2 hollow structures with enhanced lithium storage capabilities. *Nanoscale* 2011;3(5):2158–61.
- [29] Wu HB, Chen JS, Hng HH, Lou XW. Nanostructured metal oxide-based materials as advanced anodes for lithium-ion batteries. *Nanoscale* 2012;4(8):2526–42.
- [30] Hummers WS, Offeman RE. Preparation of graphitic oxide. *J Am Chem Soc* 1958;80(6):1339.
- [31] Musić S, Maljković M, Popović S, Trojko R. Formation of chromia from amorphous chromium hydroxide. *Croat Chem Acta* 1999;72(4):789–802.
- [32] Yang S, Yue WB, Zhu J, Ren Y, Yang XJ. Graphene-based mesoporous SnO_2 with enhanced electrochemical performance for lithium-ion batteries. *Adv Funct Mater* 2013;23(28):3570–6.
- [33] Balouria V, Kumar A, Singh A, Samanta S, Debnath AK, Mahajan A, et al. Temperature dependent H_2S and Cl_2 sensing selectivity of Cr_2O_3 thin films. *Sens Actuat B Chem* 2011;157(2):466–72.
- [34] Li JT, Maurice V, Swiatowska-Mrowiecka J, Seyeux A, Zanna S, Klein L, et al. XPS, time-of-flight-SIMS and polarization modulation IRRAS study of Cr_2O_3 thin film materials as anode for lithium ion battery. *Electrochim Acta* 2009;54(14):3700–7.
- [35] Zhou GM, Wang DW, Yin LC, Li N, Li F, Cheng HM. Oxygen bridges between NiO nanosheets and graphene for improvement of lithium storage. *ACS Nano* 2012;6(4):3214–23.
- [36] Vladikova D, Stoynov Z. Secondary differential impedance analysis: a tool for recognition of CPE behavior. *J Electroanal Chem* 2004;572(2):377–87.